

Interstory-interbuilding actuation schemes for seismic protection of adjacent identical buildings

Francisco Palacios-Quinonero^{*1}, Josep Rubió-Massegú¹,
Josep M. Rossell¹ and José Rodellar²

¹CoDALab, Department of Mathematics, Universitat Politècnica de Catalunya (UPC) EPSEM,
Av. Bases de Manresa 61-73, 08242 Manresa, Barcelona, Spain

²CoDALab, Department of Mathematics, Universitat Politècnica de Catalunya (UPC) EEBE,
C. Eduard Maristany 10-14, 08019 Barcelona, Spain

(Received February 28, 2019, Revised March 8, 2019, Accepted March 10, 2019)

Abstract. Rows of closely adjacent buildings with similar dynamic characteristics are common building arrangements in residential areas. In this paper, we present a vibration control strategy for the seismic protection of this kind of multibuilding systems. The proposed approach uses an advanced Linear Matrix Inequality (LMI) computational procedure to carry out the integrated design of distributed multiactuation schemes that combine interbuilding linking devices with interstory actuators implemented at different levels of the buildings. The controller designs are formulated as static output-feedback H -infinity control problems that include the interstory drifts, interbuilding approachings and control efforts as controlled-output variables. The advantages of the LMI computational procedure are also exploited to design a fully-decentralized velocity-feedback controller, which can define a passive control system with high-performance characteristics. The main ideas are presented by means of a system of three adjacent five-story identical buildings, and a proper set of numerical simulations are conducted to demonstrate the behavior of the different control configurations. The obtained results indicate that interstory-interbuilding multiactuation schemes can be used to design effective vibration control systems for adjacent buildings with similar dynamic characteristics. Specifically, this kind of control systems is able to mitigate the vibrational response of the individual buildings while maintaining reduced levels of pounding risk.

Keywords: seismic protection; identical buildings; multibuilding systems; connected control method

1. Introduction

Multibuilding systems formed by a row of closely adjacent buildings with similar dynamic characteristics is a common building arrangement in residential areas. In order to provide seismic protection to this kind of building clusters, a twofold objective needs to be considered: (i) the vibrational response of the individual buildings must be mitigated and (ii) interbuilding impacts (pounding) must be avoided. More specifically, large interstory-drift peak-values need to be suppressed and, simultaneously, interbuilding separations must be kept within safe limits. It should be noted that pounding events between closely adjacent buildings depend on the overall lateral displacement of the buildings, and can take place as the result of the cumulative effect of small interstory-drift values.

In the Connected Control Method (CCM), adjacent buildings are linked by means of interbuilding actuation devices. This idea has been extensively applied to the seismic protection of two-building systems using a wide variety of passive, semiactive and active interbuilding

linking devices. Thus, for example, studies of passive interbuilding linking devices include different kinds of fluid dampers (Xu *et al.* 1999, Zhang and Xu 2000, Yang *et al.* 2003, Cimellaro and Reinhorn 2008), viscous dampers (Bhaskararao and Jangid 2007, Patel and Jangid 2010, 2014), viscoelastic dampers (Zhang and Xu 1999, Cimellaro and Lopez-Garcia 2011, Yang and Lam 2014), friction dampers (Bhaskararao and Jangid 2006a, b) and nonlinear hysteretic devices (Ni *et al.* 2001, Basili and De Angelis 2007). Ideal semiactive links are studied by Christenson *et al.* (2007), semiactive linking devices with variable damping are proposed by Cundumi and Suárez (2008), and semiactive magnetorheological linking elements are investigated by Bharti *et al.* (2010) and Motra *et al.* (2011). The usage of shared tuned mass-dampers as linking elements are proposed by Abdullah *et al.* (2001) and Kim (2016). The effectiveness of active links are studied by Xu and Zhang (2002) and Christenson *et al.* (2003). The behavior of swing structures connected to moment-resistant frames is investigated in Jia *et al.* (2018). Additionally, hybrid control strategies that combine actuation devices implemented in the individual buildings with interbuilding actuators have been proposed to obtain an improved performance. In this line, the combined usage of base isolation systems with different kinds of dissipative linking devices are studied by Matsagar and Jangid (2005), Murase *et al.* (2013), Fathi and Bahar (2017) and Dumne *et al.*

^{*}Corresponding author, Ph.D.
E-mail: francisco.palacios@upc.edu

(2017). Hybrid actuation schemes that combine different kinds of interstory and interbuilding actuators have been proposed by Shahidzadeh *et al.* (2011), Palacios-Quinonero *et al.* (2012b, c, 2017) and Park and Ok (2015a, b).

It should be highlighted that the vast majority of the works in the literature are focused on the case of adjacent buildings with dissimilar dynamic characteristics. In this case, proper control forces can be easily generated by passive and/or semiactive interbuilding linking devices by taking advantage of the out-of-phase vibrational response of the adjacent buildings. In contrast, control strategies for seismic protection of adjacent buildings with similar dynamic characteristics have only been investigated in a reduced number of works. In this second case, the effectiveness of dissipative interbuilding links can be compromised by the synchronized vibrational response of the adjacent buildings, and more sophisticated actuation schemes are required in non-active implementations of the CCM. Two good instances of passive CCM implementations for similar adjacent buildings are the vertical cantilever linking structure presented by Makita *et al.* (2007), and the interbuilding linking schemes proposed by Patel and Jangid (2010, 2014) that implement damping links between stories located at different height levels of the adjacent buildings. Improved solutions to the problem of vibration control of adjacent buildings with similar dynamic characteristics can be obtained by considering hybrid actuation schemes, which can take advantage of the actuators implemented in the buildings to modify their dynamical response (Park and Ok 2015a, Fathi and Bahar 2017).

In this work, we investigate the effectiveness of hybrid interstory-interbuilding multiactuation schemes for the seismic protection of adjacent buildings with identical dynamic characteristics. The proposed approach uses an advanced Linear Matrix Inequality (LMI) computational procedure to carry out the integrated design of distributed high-performance multiactuation schemes that combine interbuilding linking devices with interstory actuators implemented at different levels of the buildings. The controller designs are formulated as static output-feedback H_∞ control problems (Rubio-Massegú *et al.* 2013, Palacios-Quinonero *et al.* 2014, 2016) that include the interstory drifts, interbuilding approachings and control efforts as controlled-output variables. The advantages of the LMI computational procedure are exploited to design fully-decentralized velocity-feedback controllers, which allow defining high-performance distributed actuation schemes that can be passively implemented with viscous dampers (Palacios-Quinonero *et al.* 2012a). Particular attention has been paid to the behavior of incomplete actuation schemes that include non-instrumented buildings. Also, a particular effort has been made to extend the study beyond the two-building configuration. Thus, a general formulation of the multibuilding problem is provided, and a particular system of three adjacent five-story identical buildings is used in the controller designs and numerical simulations (see Fig. 1). This multibuilding layout makes it possible to carry out a detailed discussion of the main elements and, at the same time, provides a clear portrait of the richness and complexity of the considered problem. Specifically, two

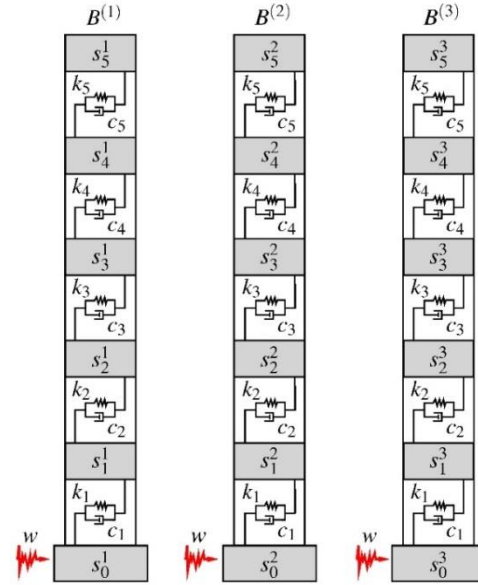


Fig. 1 Uncontrolled multibuilding system formed by three five-story identical buildings

different interstory actuation schemes are discussed: (i) a *one-sided actuation scheme* with interstory actuation devices implemented only in one of the external buildings (see Fig. 4) and (ii) a *two-sided actuation scheme* with interstory actuation devices implemented in both external buildings (see Fig. 9). These interstory actuation schemes are complemented with interbuilding actuation devices to define high-performance hybrid interstory-interbuilding control strategies for the seismic protection of the overall multibuilding system (see Figs. 5 and 10). To demonstrate the behavior of the different control configurations, a proper set of numerical simulations are conducted using the full-scale North-South El Centro 1940 seismic record as ground-acceleration input (see Fig. 2).

The rest of the paper is organized as follows: In Section 2, a general dynamical model for systems of adjacent identical buildings is provided. The design and performance of linked and unlinked one-sided actuation schemes are considered in Section 3. Two-sided actuation schemes are examined in Section 4. Some conclusions and future research lines are briefly discussed in Section 5. Finally, a summary of the LMI controller-design procedure and the particular values of the building parameters used in the controller designs and numerical simulations are collected in the appendices.

2. Mathematical model

2.1 Uncontrolled system

Let us consider a system of n_b adjacent identical buildings as the three-building system schematically depicted in Fig. 1. The lateral motion of the j th building $B^{(j)}$ can be described by the second order differential equation

$$\tilde{M}\ddot{q}^{(j)}(t) + \tilde{C}_d\dot{q}^{(j)}(t) + \tilde{K}q^{(j)}(t) = \tilde{T}_w w(t) \quad (1)$$

where

$$q^{(j)}(t) = [q_1^j(t), \dots, q_{n_s}^j(t)]^T \quad (2)$$

is the vector of story displacements of building $B^{(j)}$, $q_i^j(t)$ is the displacement of the i th story (denoted as s_i^j in Fig. 1) with respect to the building ground level s_0^j , n_s is the number of stories, $\tilde{M} \in \mathbb{R}^{n_s \times n_s}$ is the building mass matrix, $\tilde{C}_d \in \mathbb{R}^{n_s \times n_s}$ is the building damping matrix, $\tilde{K} \in \mathbb{R}^{n_s \times n_s}$ is the building stiffness matrix, $w(t) \in \mathbb{R}$ is the ground-acceleration disturbance and $\tilde{T}_w \in \mathbb{R}^{n_s \times 1}$ is the building disturbance-input matrix. The building mass matrix has the diagonal form

$$\tilde{M} = \begin{bmatrix} m_1 & & \\ & \ddots & \\ & & m_{n_s} \end{bmatrix} \quad (3)$$

where m_i is the mass of the i th story, and the building stiffness matrix has the following tridiagonal structure

$$\tilde{K} = \begin{bmatrix} k_1 + k_2 & -k_2 & 0 & & \\ -k_2 & k_2 + k_3 & -k_3 & & \\ & \ddots & \ddots & \ddots & \\ & -k_{n_s-1} & k_{n_s-1} + k_{n_s} & -k_{n_s} & \\ 0 & & -k_{n_s} & k_{n_s} & \end{bmatrix} \quad (4)$$

where k_i is the stiffness coefficient of the i th story. When the values of the story damping coefficients c_i are known, a building damping matrix \tilde{C}_d with the tridiagonal structure in Eq. (4) can be computed by substituting the stiffness coefficients k_i by the corresponding damping coefficients c_i , $i = 1, \dots, n_s$. Quite frequently, however, it is not possible to properly determine the values of the story damping coefficients and an approximate building damping matrix is computed using other computational methods (Chopra 2017). The particular values of the matrices \tilde{M} , \tilde{C}_d and \tilde{K} used in the numerical simulations and controller designs discussed in this paper are collected in Appendix B. The building disturbance-input matrix has the following form

$$\tilde{T}_w = -\tilde{M} [1]_{n_s \times 1} \quad (5)$$

where $[1]_{m \times n}$ denotes a matrix of dimensions $m \times n$ with all its entries equal to one.

A more convenient description of the vibrational response of building $B^{(j)}$ can be obtained by considering the vector of interstory drifts

$$r^{(j)}(t) = [r_1^j(t), \dots, r_{n_s}^j(t)]^T \quad (6)$$

where $r_i^j(t)$ is the relative displacement between the consecutive stories s_i^j and s_{i-1}^j of $B^{(j)}$, which can be defined as

$$\begin{cases} r_1^j(t) = q_1^j(t), \\ r_i^j(t) = q_i^j(t) - q_{i-1}^j(t), \quad 1 < i \leq n_s \end{cases} \quad (7)$$

The vector of interstory drifts of $B^{(j)}$ can be computed in the form

$$r^{(j)}(t) = \tilde{C}_r q^{(j)}(t) \quad (8)$$

where the matrix $\tilde{C}_r \in \mathbb{R}^{n_s \times n_s}$ has the following lower-diagonal band structure

$$\tilde{C}_r = \begin{bmatrix} 1 & & & \\ -1 & 1 & & \\ & \ddots & \ddots & \\ & & -1 & 1 \\ & & & -1 & 1 \end{bmatrix} \quad (9)$$

The possible interaction between the adjacent buildings $B^{(j)}$ and $B^{(j+1)}$ can be modeled using the vector of interbuilding approachings

$$\begin{aligned} a^{(j)}(t) &= [a_1^j(t), \dots, a_{n_s}^j(t)]^T \\ &\triangleq -(q^{(j+1)}(t) - q^{(j)}(t)) \end{aligned} \quad (10)$$

where the element $a_i^j(t)$ describes the approaching between the stories s_i^j and s_i^{j+1} placed at the i th level in the adjacent buildings $B^{(j)}$ and $B^{(j+1)}$. It should be noted that, due to the initial negative sign, a positive value of the interbuilding approaching $a_i^j(t)$ corresponds to a reduction in the interbuilding separation between the stories s_i^j and s_i^{j+1} . The maximum approaching peak-value

$$a_{\max}^{(j)} = \max_{1 \leq i \leq n_s} \left(\max_{0 \leq t \leq T} a_i^j(t) \right) \quad (11)$$

indicates the maximum reduction of the interbuilding separation between buildings $B^{(j)}$ and $B^{(j+1)}$ in the time interval $[0, T]$. To avoid the huge computational complexity associated to interbuilding collisions (Khatiwada and Chouw 2014, Kharazian and López-Almansa 2019, Shi *et al.* 2018, Bamer *et al.* 2018, Impollonia and Palmeri 2018, Chinmayi 2019), the numerical simulations presented in this paper are carried out assuming that the interbuilding gap is large enough to prevent pounding. In this context, $a_{\max}^{(j)}$ can be understood as a lower bound of safe interbuilding gap between $B^{(j)}$ and $B^{(j+1)}$.

The overall dynamical response of the uncontrolled multi-building system can be described by the second-order differential equation

$$M\ddot{q}(t) + C_d \dot{q}(t) + Kq(t) = T_w w(t) \quad (12)$$

where $q(t) \in \mathbb{R}^n$ is the overall vector of story displacements

$$q(t) = [\{q^{(1)}(t)\}^T, \dots, \{q^{(n_b)}(t)\}^T]^T \quad (13)$$

$n = n_b \times n_s$ is the total number of degrees of freedom; $M \in \mathbb{R}^{n \times n}$, $C_d \in \mathbb{R}^{n \times n}$, $K \in \mathbb{R}^{n \times n}$ are the overall mass, damping and stiffness matrices, respectively; and $T_w \in \mathbb{R}^{n \times 1}$ is the overall disturbance-input matrix. The matrices M , C_d and K have the following block-diagonal structure

$$M = \begin{bmatrix} \tilde{M} & & \\ & \ddots & \\ & & \tilde{M} \end{bmatrix}, C_d = \begin{bmatrix} \tilde{C}_d & & \\ & \ddots & \\ & & \tilde{C}_d \end{bmatrix}, K = \begin{bmatrix} \tilde{K} & & \\ & \ddots & \\ & & \tilde{K} \end{bmatrix} \quad (14)$$

and T_w can be written in the form

$$T_w = -M[1]_{n \times 1} \quad (15)$$

The overall vector of interstory drifts

$$r(t) = [\{r^{(1)}(t)\}^T, \dots, \{r^{(n_b)}(t)\}^T]^T \quad (16)$$

can be computed as

$$r(t) = C_r q(t) \quad (17)$$

where the matrix $C_r \in \mathbb{R}^{n \times n}$ has the following block-diagonal structure

$$C_r = \begin{bmatrix} \tilde{C}_r & & \\ & \ddots & \\ & & \tilde{C}_r \end{bmatrix} \quad (18)$$

and \tilde{C}_r is the local interstory output-matrix defined in Eq. (9). Finally, the overall vector of interbuilding approachings

$$a(t) = [\{a^{(1)}(t)\}^T, \dots, \{a^{(n_b-1)}(t)\}^T]^T \quad (19)$$

has dimension $n_a = (n_b - 1) n_s$ and can be computed as

$$a(t) = C_a q(t) \quad (20)$$

using the matrix $C_a \in \mathbb{R}^{n_a \times n}$ with the following band-diagonal block structure

$$C_a = \begin{bmatrix} I_{n_s} & -I_{n_s} & & \\ & I_{n_s} & -I_{n_s} & \\ & & \dots & \dots \\ & & & I_{n_s} & -I_{n_s} \end{bmatrix} \quad (21)$$

where I_n denotes an identity matrix of dimension n . For the three-building system in Fig. 1, the overall vector of interbuilding approachings

$$a(t) = [\{a^{(1)}(t)\}^T, \{a^{(2)}(t)\}^T]^T \quad (22)$$

has dimension $n_a = 10$ and the corresponding matrix C_a has the form

$$C_a = \begin{bmatrix} I_5 & -I_5 & [0]_{5 \times 5} \\ [0]_{5 \times 5} & I_5 & -I_5 \end{bmatrix} \quad (23)$$

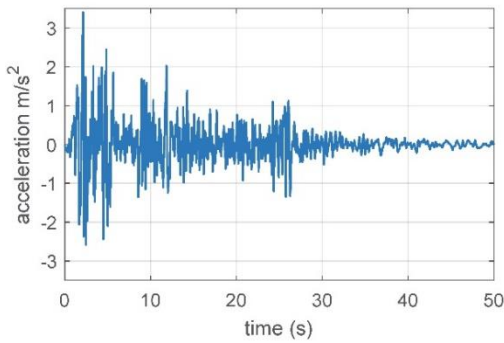


Fig. 2 Full-scale North-South El Centro 1940 accelerogram

where $[0]_{m \times n}$ is a null matrix of dimensions $m \times n$. The uncontrolled seismic response of this multibuilding system corresponding to the building parameters presented in Appendix B and the full-scale North-South El Centro 1940 ground acceleration seismic record (see Fig. 2) are presented in Fig. 3, where the plots in Figs. 3(a)-3(c) display the maximum absolute values attained by the components of the interstory-drift vectors $r^{(1)}(t)$, $r^{(2)}(t)$ and $r^{(3)}(t)$, respectively, and the plots in Figs. 3(d) and 3(e) show the maximum values reached by the components of the interbuilding-approaching vectors $a^{(1)}(t)$ and $a^{(2)}(t)$, respectively. The plots in the upper Figs. 3(a)-3(c) demonstrate the identical dynamical characteristics of the buildings and indicate that a maximum interstory-drift peak-value of about 5.3 cm is produced at the buildings' second-story level. The plots in the lower Figs. 3(d)-3(e) illustrate the null interbuilding-approaching peak-values produced by the synchronized vibrational response of the identical buildings.

2.2 Controlled system

To describe the seismic response of controlled multibuilding systems, as those schematically depicted in Figs. 4, 5, 9 and 10, we consider the second-order differential equation

$$M\ddot{q}(t) + C_d \dot{q}(t) + Kq(t) = T_u u(t) + T_w w(t) \quad (24)$$

where $u(t) \in \mathbb{R}^{n_u}$ is the vector of control actions, n_u is the overall number of actuation devices and $T_u \in \mathbb{R}^{n \times n_u}$ is the control-input matrix, which can be written in the following form

$$T_u = \begin{bmatrix} T_u^{(1)} \\ \vdots \\ T_u^{(n_b)} \end{bmatrix} \quad (25)$$

where $T_u^{(j)} \in \mathbb{R}^{n_s \times n_u}$ is a matrix that models the effect of the overall actuation system on building $B^{(j)}$. Thus, for example, the unlinked one-sided actuation scheme of the controlled three-building system in Fig. 4 includes four interstory force-actuation devices implemented at the bottom levels of building $B^{(1)}$. In this case, we have $n_u = 4$ and the control-input matrix is

$$\{T_u\}_1 = \begin{bmatrix} \{T_u^{(1)}\}_1 \\ [0]_{5 \times 4} \\ [0]_{5 \times 4} \end{bmatrix} \quad (26)$$

with

$$\{T_u^{(1)}\}_1 = \begin{bmatrix} 1 & -1 & 0 & 0 \\ 0 & 1 & -1 & 0 \\ 0 & 0 & 1 & -1 \\ 0 & 0 & 0 & 1 \\ 0 & 0 & 0 & 0 \end{bmatrix} \quad (27)$$

For the controlled system in Fig. 5, the actuation scheme includes four interstory actuation devices implemented in $B^{(1)}$ plus two interbuilding actuators: d_5 that links $B^{(1)}$ and $B^{(2)}$ at the fourth story level, and d_6 that links $B^{(2)}$

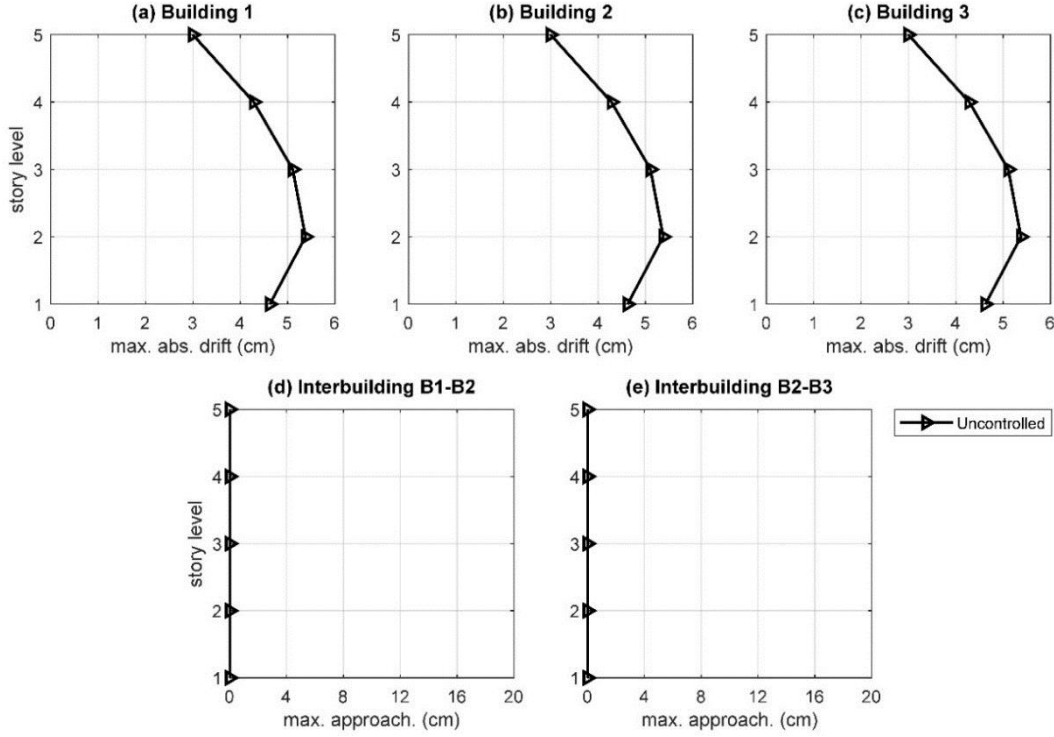


Fig. 3 Time response of the uncontrolled three-building system: (a) maximum absolute interstory-drift values of building 1, (b) maximum absolute interstory-drift values of building 2, (c) maximum absolute interstory-drift values of building 3, (d) maximum interbuilding approachings between buildings 1 and 2, (e) maximum interbuilding approachings between buildings 2 and 3. The full-scale North-South 1940 ground acceleration record has been used as seismic disturbance

and $B^{(3)}$ at the third story level. In this case, the overall number of actuation devices is $n_u = 6$ and the structure of the control-input matrix is

$$\{T_u\}_{II} = \begin{bmatrix} \{T_u^{(1)}\}_{II} \\ \{T_u^{(2)}\}_{II} \\ \{T_u^{(3)}\}_{II} \end{bmatrix} \quad (28)$$

with

$$\{T_u^{(1)}\}_{II} = \begin{bmatrix} 1 & -1 & 0 & 0 & 0 & 0 \\ 0 & 1 & -1 & 0 & 0 & 0 \\ 0 & 0 & 1 & -1 & 0 & 0 \\ 0 & 0 & 0 & 1 & -1 & 0 \\ 0 & 0 & 0 & 0 & 0 & 0 \end{bmatrix} \quad (29)$$

$$\{T_u^{(2)}\}_{II} = \begin{bmatrix} 0 & 0 & 0 & 0 & 0 & 0 \\ 0 & 0 & 0 & 0 & 0 & 0 \\ 0 & 0 & 0 & 0 & 0 & -1 \\ 0 & 0 & 0 & 0 & 1 & 0 \\ 0 & 0 & 0 & 0 & 0 & 0 \end{bmatrix} \quad (30)$$

$$\{T_u^{(3)}\}_{II} = \begin{bmatrix} 0 & 0 & 0 & 0 & 0 & 0 \\ 0 & 0 & 0 & 0 & 0 & 0 \\ 0 & 0 & 0 & 0 & 0 & 1 \\ 0 & 0 & 0 & 0 & 0 & 0 \\ 0 & 0 & 0 & 0 & 0 & 0 \end{bmatrix} \quad (31)$$

By considering the state vector

$$x(t) = \begin{bmatrix} q(t) \\ \dot{q}(t) \end{bmatrix} \quad (32)$$

we can obtain a first-order state-space model

$$\dot{x}(t) = A x(t) + B u(t) + E w(t) \quad (33)$$

$$A = \begin{bmatrix} [0]_{n \times n} & I_n \\ -M^{-1}K & -M^{-1}C_d \end{bmatrix} \quad (34)$$

$$B = \begin{bmatrix} [0]_{n \times n_u} \\ M^{-1}T_u \end{bmatrix}, \quad E = \begin{bmatrix} [0]_{n \times 1} \\ -[1]_{n \times 1} \end{bmatrix} \quad (35)$$

The overall vector of interstory drifts can be computed from the state vector in the form

$$r(t) = \hat{C}_r x(t) \quad (36)$$

where $\hat{C}_r \in \mathbb{R}^{n \times 2n}$ has the block structure

$$\hat{C}_r = [C_r \quad 0]_{n \times n} \quad (37)$$

and C_r is the matrix defined in Eq. (18). Analogously, the overall vector of interbuilding approachings can be computed in the form

$$a(t) = \hat{C}_a x(t) \quad (38)$$

where $\hat{C}_a \in \mathbb{R}^{n_a \times 2n}$ has the block structure

$$\hat{C}_a = [C_a \quad 0]_{n_a \times n} \quad (39)$$

and C_a is the matrix defined in Eq. (21).

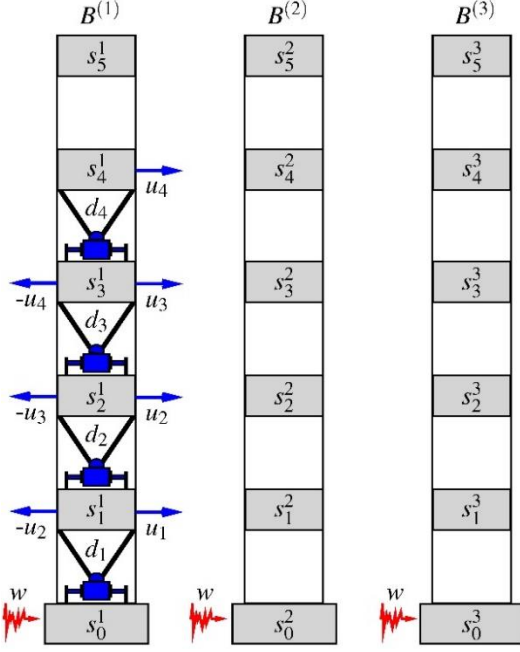


Fig. 4 Unlinked one-sided actuation scheme AS1. Controlled multibuilding system with four interstory actuators implemented in building $B^{(1)}$. Buildings $B^{(2)}$ and $B^{(3)}$ are non-instrumented unlinked buildings

3. One-sided actuation schemes

In this section, we consider the actuation schemes AS1 and AS2 schematically depicted in Figs.4 and 5, respectively. These actuation schemes contain a set of ideal force-actuation devices implemented at selected places of the multibuilding structure. The actuation devices can be of two different kinds: *interstory actuators*, which are implemented between consecutive stories of the same building, and *interbuilding actuators*, which are allocated between adjacent stories of neighboring buildings. Buildings with no interstory actuators are considered non-instrumented, as the control system implementation could be carried out with minor impact on these buildings. Buildings that are not affected by interbuilding actuators are called unlinked. Linked actuation schemes contain only linked buildings; otherwise, the actuation scheme is unlinked. The actuation schemes AS1 and AS2 comprise one instrumented building and two non-instrumented buildings. AS2 is a linked scheme and AS1 is unlinked.

As schematically indicated in the figures, the actuator d_i produces a pair of opposite forces of magnitude $|u_i(t)|$ on the associated stories. We also assume that each actuation device incorporates a collocated sensor that provides the relative velocity of the stories associated to the actuator. For a given control configuration, we want to design a static output-feedback controller of the form

$$u(t) = Gy(t) \quad (40)$$

where $u(t) \in \mathbb{R}^{n_u}$ is the vector of control actions, $y(t) \in \mathbb{R}^{n_y}$ is the vector of measured outputs and $G \in \mathbb{R}^{n_u \times n_y}$ is a constant control gain matrix. The unlinked

actuation scheme AS1 includes four interstory force-actuation devices $d_i, i = 1, \dots, 4$, implemented at the lowest levels of the instrumented building $B^{(1)}$. The seismic response of the controlled three-building system with this actuation scheme can be described by the state-space model given in Eq. (33) with the control vector

$$u_1(t) = [u_1(t), u_2(t), u_3(t), u_4(t)]^T \quad (41)$$

and the control-input matrix $\{T_u\}_1$ given in Eqs. (26)-(27). In this case, we want to design a static output-feedback controller

$$u_1(t) = G_1 y_1(t) \quad (42)$$

that computes the control actions from the feedback information provided by the vector of measured outputs

$$y_1(t) = [\dot{r}_1^1(t), \dot{r}_2^1(t), \dot{r}_3^1(t), \dot{r}_4^1(t)]^T \quad (43)$$

which contains the interstory velocities corresponding to the instrumented levels of $B^{(1)}$. Using the state vector $x(t)$ in Eq. (32), $y_1(t)$ can be written in the form

$$y_1(t) = \{C_y\}_1 x(t) \quad (44)$$

with the observed-output matrix

$$\{C_y\}_1 = \begin{bmatrix} [0]_{4 \times 15} & \{T_u\}_1^T \end{bmatrix} \quad (45)$$

where $\{T_u\}_1^T$ is the transpose of the control-input matrix. Assuming that the controller design objectives are mitigating the buildings vibrational response and reducing the risk of pounding events by means of moderate control efforts, we consider a controlled-output vector that includes the overall interstory drifts, interbuilding approachings and control efforts

$$z(t) = \begin{bmatrix} \alpha_r r(t) \\ \alpha_a a(t) \\ \alpha_u u(t) \end{bmatrix} \quad (46)$$

where α_r , α_a and α_u are suitable scaling factors. Using the matrices \hat{C}_r and \hat{C}_a defined in Eqs.(37) and (39), respectively, the vector of controlled outputs can be written in the form

$$z(t) = C_z x(t) + D_z u(t) \quad (47)$$

where

$$C_z = \begin{bmatrix} \alpha_r \hat{C}_r \\ \alpha_a \hat{C}_a \\ [0]_{n_u \times 2n} \end{bmatrix}, D_z = \begin{bmatrix} [0]_{3n_s \times n_u} \\ [0]_{2n_s \times n_u} \\ \alpha_u I_{n_u} \end{bmatrix} \quad (48)$$

To compute the gain matrix G_1 in Eq. (42), we apply the LMI controller design procedure presented in Appendix A with the system matrices A , B and E in Eqs.(34) and (35) corresponding to the building matrices \tilde{M} , \tilde{K} and \tilde{C}_d given in Appendix B and the control-input matrix $\{T_u\}_1$; the observed-output matrix $\{C_y\}_1$ in Eq. (45); and the controlled-output matrices C_z and D_z in Eq.(48) with $n_u = 4$, $n = 15$, $n_s = 5$ and the scaling factors

$$\alpha_r = 15, \quad \alpha_a = 1, \quad \alpha_u = 10^{-7.4} \quad (49)$$

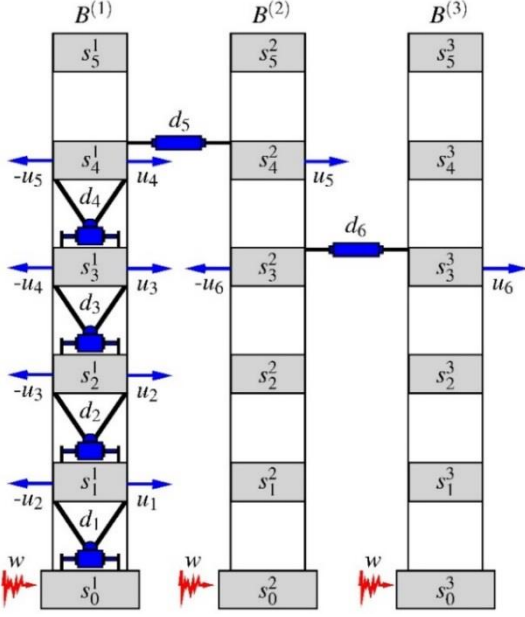


Fig. 5 Linked one-sided actuation scheme AS2. Controlled multibuilding system with four interstory actuators implemented in building $B^{(1)}$ and two linking interbuilding actuators. Buildings $B^{(2)}$ and $B^{(3)}$ are non-instrumented linked buildings

As a result, we obtain the control gain matrix

$$G_1 = 10^6 \times \begin{bmatrix} -9.089 & -7.639 & -4.833 & -0.844 \\ -6.582 & -6.611 & -5.104 & -1.402 \\ -4.990 & -4.284 & -4.235 & -2.550 \\ -4.369 & -3.662 & -2.268 & -1.843 \end{bmatrix} \quad (50)$$

Next, we consider the linked one-sided actuation scheme AS2 displayed in Fig. 5, which includes two additional interbuilding actuators: d_5 that links $B^{(1)}$ and $B^{(2)}$ at the fourth story level, and d_6 that links $B^{(2)}$ and $B^{(3)}$ at the third story level. In this case, the overall control vector $u_{II}(t)$ contains two new components $u_5(t)$ and $u_6(t)$, which indicate the control actions corresponding to the interbuilding actuators d_5 and d_6 , respectively. Analogously, the observed-output vector $y_{II}(t) \in \mathbb{R}^6$ contains the interstory velocities

$$y_i(t) = \dot{r}_i^1(t), \quad i = 1, \dots, 4 \quad (51)$$

plus the relative interbuilding velocities

$$y_5(t) = \dot{q}_4^2(t) - \dot{q}_4^1(t), \quad y_6(t) = \dot{q}_3^3(t) - \dot{q}_3^2(t) \quad (52)$$

The control-input matrix $\{T_u\}_{II}$ corresponding to this actuation scheme has the form indicated in Eqs. (28)-(31), and the observed-output matrix can be written as

$$\{C_y\}_{II} = \begin{bmatrix} [0]_{6 \times 15} & \{T_u\}_{II}^T \end{bmatrix} \quad (53)$$

By applying the LMI controller design procedure with the same building parameters, the matrices $\{T_u\}_{II}$ and $\{C_y\}_{II}$, and the controlled-output matrices C_z and D_z in Eq. (48) with dimensions $n_u = 6$, $n = 15$, $n_s = 5$ and the scaling factors in Eq. (49), we obtain a static velocity-feedback controller

$$u_{II}(t) = G_{II} y_{II}(t) \quad (54)$$

with the control gain matrix presented in Fig. 6.

To illustrate the behavior of the proposed control configurations, we have conducted a set of numerical simulations using the full-scale North-South El Centro 1940 seismic record as ground acceleration disturbance. The obtained results are presented in Fig. 7, where the dashed green lines with asterisks display the response of the unlinked actuation scheme AS1 with the velocity-feedback controller $u_I(t) = G_I y_I(t)$, the solid red lines with squares show the response of the linked actuation scheme AS2 with the velocity-feedback controller $u_{II}(t) = G_{II} y_{II}(t)$, and the solid black lines with triangles present the uncontrolled response. The control-effort peak-values corresponding to the different actuation devices are displayed in Fig. 8, where the plain green bars represent the unlinked actuation scheme AS1 and the red bars with dashed pattern correspond to the linked actuation scheme AS2.

Looking at the upper plots in Figs. 7(a)-7(c), it can be appreciated that the unlinked actuation scheme AS1 provides a significant reduction of the interstory-drift peak-values in the instrumented building $B^{(1)}$ but it is totally ineffective on the non-instrumented buildings $B^{(2)}$ and $B^{(3)}$. Moreover, the plots in Fig. 7(d) clearly indicate that the actuation scheme AS1 can have a detrimental effect on the interbuilding pounding by producing interbuilding approaches of more than 16 cm between buildings $B^{(1)}$ and $B^{(2)}$. Looking at the plots corresponding to the actuation scheme AS2, it can be appreciated that this linked configuration provides a relevant reduction of the interstory-drift peak-values in all the buildings, with maximum interbuilding approaches that are small between buildings $B^{(1)}$ and $B^{(2)}$ (less than 2 cm) and moderate between buildings $B^{(2)}$ and $B^{(3)}$ (less than 5 cm). The overall performance of the actuation scheme AS1 is clearly unsatisfactory as it produces only a partial reduction of the vibrational response and increases the pounding risk. In contrast, the linked control configuration AS2 provides an overall mitigation of the buildings vibrational response with a reduced risk of pounding. However, it should be noted that the overall vibration control of the multibuilding system attained by the linked configuration AS2 produces also a remarkable increase of the control-effort peak-values, which can be clearly appreciated in Fig. 8.

Remark 1. The proposed velocity-feedback controllers can operate with the partial state information provided by the system of collocated sensors. However, these controllers are centralized, in the sense that the complete observed-output vector is required to compute the control actions. For a linked actuation scheme, this fact implies that a wide communication system covering the overall multibuilding structure will be required to implement the control system.

Remark 2. Looking at the solid black lines with triangles in Figs. 7(d)-7(e), it can be observed that the interbuilding approaches produced by the uncontrolled system are null. This fact is the result of the synchronized dynamical response of the idealized multibuilding model and implies

$$G_{II} = 10^6 \times \begin{bmatrix} -1.463 & -1.220 & -0.807 & -0.388 & -0.026 & -0.098 \\ -1.188 & -1.180 & -0.927 & -0.531 & -0.094 & -0.073 \\ -1.016 & -0.960 & -0.943 & -0.697 & -0.206 & -0.023 \\ -0.809 & -0.774 & -0.728 & -0.722 & -0.409 & 0.020 \\ -0.587 & -0.594 & -0.596 & -0.569 & -0.633 & -0.012 \\ -0.095 & -0.104 & -0.117 & -0.116 & -0.073 & -0.388 \end{bmatrix}$$

Fig. 6 Gain matrix for the static output-feedback controller $u_{II}(t) = G_{II} y_{II}(t)$

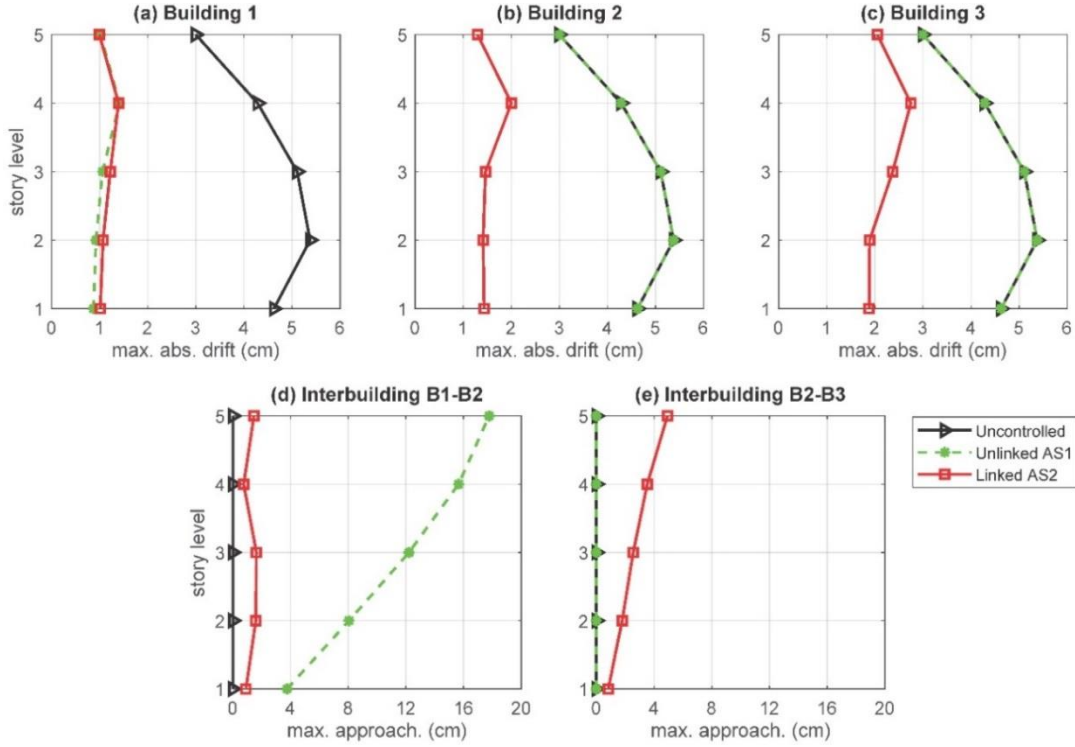


Fig. 7 Time response of the controlled three-building system corresponding to the unlinked actuation scheme AS1 with the control matrix G_I (dashed green line with asterisks) and the linked actuation scheme AS2 with the control matrix G_{II} (solid red line with squares): (a) maximum absolute interstory-drift values of building 1, (b) maximum absolute interstory-drift values of building 2, (c) maximum absolute interstory-drift values of building 3, (d) maximum interbuilding approachings between buildings 1 and 2, (e) maximum interbuilding approachings between buildings 2 and 3. The solid black line with triangles corresponds to the uncontrolled system

that the pounding risk in the free response is null. In this sense, the action of the control system defined by the linked configuration AS2 can produce an increment of the pounding risk. The data obtained in the numerical simulations indicate that the interbuilding approachings produced by the actuation scheme AS2 are all inferior to 5 cm. This means that, for the considered seismic excitation, no pounding events would have been taken place in this case with an interbuilding separation gap of 5 cm.

4. Two-sided actuation schemes

In this section, we consider the actuation schemes AS3 and AS4 schematically depicted in Figs. 9 and 10, respectively. The unlinked scheme AS3 contains six interstory actuators implemented in the first three story-

levels of the external buildings $B^{(1)}$ and $B^{(3)}$. The control-input matrix for this actuation scheme has the form

$$\{T_u\}_{III} = \begin{bmatrix} \{T_u^{(1)}\}_{III} \\ [0]_{5 \times 6} \\ \{T_u^{(3)}\}_{III} \end{bmatrix} \quad (55)$$

with

$$\{T_u^{(1)}\}_{III} = \begin{bmatrix} 1 & -1 & 0 & 0 & 0 & 0 \\ 0 & 1 & -1 & 0 & 0 & 0 \\ 0 & 0 & 1 & 0 & 0 & 0 \\ 0 & 0 & 0 & 0 & 0 & 0 \\ 0 & 0 & 0 & 0 & 0 & 0 \end{bmatrix} \quad (56)$$

$$\{T_u^{(3)}\}_{III} = \begin{bmatrix} 0 & 0 & 0 & 1 & -1 & 0 \\ 0 & 0 & 0 & 0 & 1 & -1 \\ 0 & 0 & 0 & 0 & 0 & 1 \\ 0 & 0 & 0 & 0 & 0 & 0 \\ 0 & 0 & 0 & 0 & 0 & 0 \end{bmatrix} \quad (57)$$

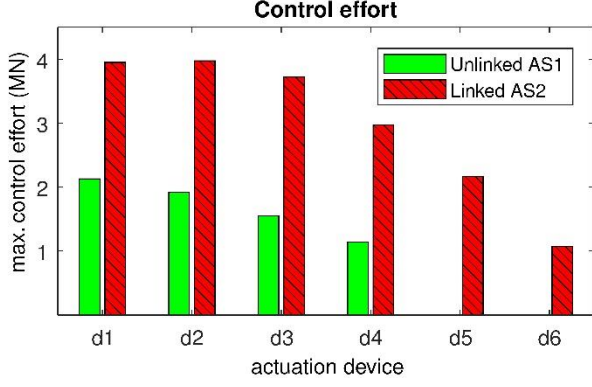


Fig. 8 Control-effort peak-values (MN) corresponding to the unlinked actuation scheme AS1 with the control matrix G_I (plain green bars) and the linked actuation scheme AS2 with the control matrix G_{II} (red bars with dashed pattern)

The observed-output vector $y_{III}(t) \in \mathbb{R}^6$ that contains the interstory velocities provided by the collocated sensors has the following components

$$\begin{cases} y_i(t) = \dot{r}_i^1(t), & i = 1, 2, 3 \\ y_i(t) = \dot{r}_{i-3}^3(t), & i = 4, 5, 6 \end{cases} \quad (58)$$

and can be computed as

$$y_{III}(t) = \{C_y\}_{III} x(t) \quad (59)$$

with the observed-output matrix

$$\{C_y\}_{III} = \begin{bmatrix} [0]_{6 \times 15} & \{T_u\}_{III}^T \end{bmatrix} \quad (60)$$

Considering the controlled-output matrices C_z and D_z in Eq. (48) with proper dimensions and the scaling factors given in Eq. (49), and following the same controller design procedure used in the previous section, we obtain a velocity-feedback controller

$$u_{III}(t) = G_{III} y_{III}(t) \quad (61)$$

for the actuation scheme AS3 with the control gain matrix G_{III} presented in Fig. 11. The linked actuation scheme AS4 includes two additional interbuilding actuators that link the buildings at the four-story level. The corresponding control-input matrix has the form

$$\{T_u\}_{IV} = \begin{bmatrix} \{T_u^{(1)}\}_{IV} \\ \{T_u^{(2)}\}_{IV} \\ \{T_u^{(3)}\}_{IV} \end{bmatrix} \quad (62)$$

with

$$\{T_u^{(1)}\}_{IV} = \begin{bmatrix} 1 & -1 & 0 & 0 & 0 & 0 & 0 & 0 \\ 0 & 1 & -1 & 0 & 0 & 0 & 0 & 0 \\ 0 & 0 & 1 & 0 & 0 & 0 & 0 & 0 \\ 0 & 0 & 0 & 0 & 0 & 0 & -1 & 0 \\ 0 & 0 & 0 & 0 & 0 & 0 & 0 & 0 \end{bmatrix} \quad (63)$$

$$\{T_u^{(2)}\}_{IV} = \begin{bmatrix} 0 & 0 & 0 & 0 & 0 & 0 & 0 & 0 \\ 0 & 0 & 0 & 0 & 0 & 0 & 0 & 0 \\ 0 & 0 & 0 & 0 & 0 & 0 & 1 & -1 \\ 0 & 0 & 0 & 0 & 0 & 0 & 0 & 0 \end{bmatrix} \quad (64)$$

$$\{T_u^{(3)}\}_{IV} = \begin{bmatrix} 0 & 0 & 0 & 1 & -1 & 0 & 0 & 0 \\ 0 & 0 & 0 & 0 & 1 & -1 & 0 & 0 \\ 0 & 0 & 0 & 0 & 0 & 1 & 0 & 0 \\ 0 & 0 & 0 & 0 & 0 & 0 & 0 & 1 \\ 0 & 0 & 0 & 0 & 0 & 0 & 0 & 0 \end{bmatrix} \quad (65)$$

and the observed-output vector $y_{IV}(t) \in \mathbb{R}^8$ contains the six initial components indicated in Eq. (58) plus the inter-building velocities

$$y_7(t) = \dot{q}_4^2(t) - \dot{q}_4^1(t), \quad y_8(t) = \dot{q}_4^3(t) - \dot{q}_4^2(t) \quad (66)$$

For the actuation scheme AS4, following the same control design procedure used in the previous cases, we obtain a velocity-feedback controller

$$u_{IV}(t) = G_{IV} y_{IV}(t) \quad (67)$$

with the gain matrix G_{IV} displayed in Fig. 11. Additionally, we take advantage of the possibility of setting sparsity patterns on the optimization matrices provided by the LMI solvers and, by constraining the matrices X_R and Y_R to diagonal form in the LMI optimization problem \mathcal{P}_2 given in Eq. (73), we obtain for AS4 a fully-decentralized velocity-feedback controller

$$\hat{u}_{IV}(t) = \hat{G}_{IV} y_{IV}(t) \quad (68)$$

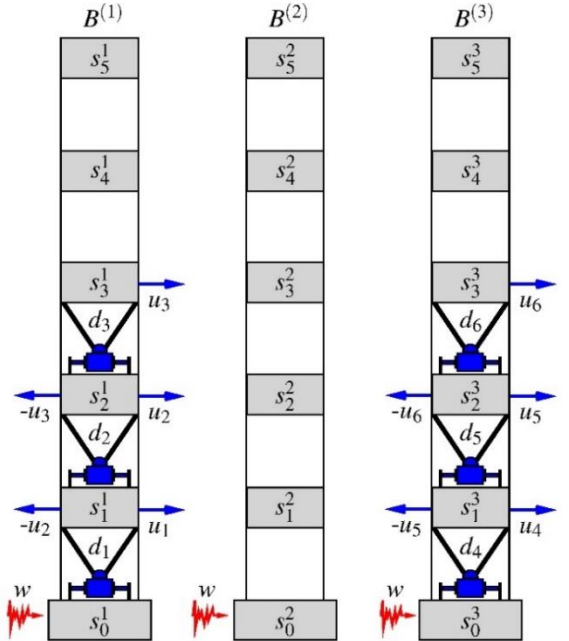


Fig. 9 Unlinked actuation scheme AS3. Controlled multi-building system with three interstory actuators implemented in buildings $B^{(1)}$ and $B^{(3)}$. The building $B^{(2)}$ is a non-instrumented unlinked building

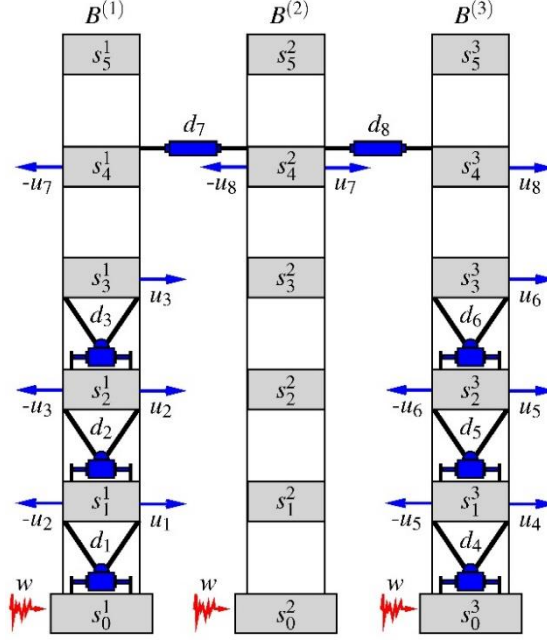


Fig. 10 Linked actuation scheme AS4. Controlled multibuilding system with three interstory actuators implemented in the lateral buildings $B^{(1)}$ and $B^{(3)}$ and two linking interbuilding actuators

$$G_{\text{III}} = 10^6 \times \begin{bmatrix} -7.174 & -5.459 & -3.054 & -0.710 & -0.405 & 0.187 \\ -4.406 & -4.489 & -3.537 & -0.602 & -0.394 & -0.019 \\ -2.139 & -1.082 & -2.272 & -0.888 & -0.590 & -0.185 \\ -0.658 & -0.466 & 0.234 & -7.181 & -5.472 & -3.056 \\ -0.649 & -0.431 & 0.039 & -4.404 & -4.493 & -3.539 \\ -0.864 & -0.531 & -0.168 & -2.140 & -1.083 & -2.275 \end{bmatrix}$$

$$G_{\text{IV}} = 10^7 \times \begin{bmatrix} -1.061 & -0.863 & -0.425 & -0.334 & -0.278 & -0.106 & 0.362 & 0.190 \\ -0.618 & -0.681 & -0.486 & -0.206 & -0.192 & -0.148 & 0.316 & 0.176 \\ -0.312 & -0.278 & -0.324 & -0.071 & -0.052 & -0.061 & 0.211 & 0.171 \\ -0.353 & -0.260 & -0.069 & -1.058 & -0.852 & -0.404 & -0.175 & -0.367 \\ -0.185 & -0.166 & -0.118 & -0.609 & -0.668 & -0.470 & -0.176 & -0.312 \\ -0.042 & -0.026 & -0.044 & -0.307 & -0.270 & -0.316 & -0.158 & -0.202 \\ -0.185 & -0.190 & -0.184 & 0.099 & 0.057 & -0.001 & -0.265 & 0.002 \\ -0.109 & -0.067 & -0.016 & 0.176 & 0.176 & 0.166 & 0.000 & -0.265 \end{bmatrix}$$

Fig. 11 Gain matrices for the static output-feedback controllers $u_{\text{III}}(t) = G_{\text{III}} y_{\text{III}}(t)$ and $u_{\text{IV}}(t) = G_{\text{IV}} y_{\text{IV}}(t)$

with a diagonal control gain matrix \hat{G}_{IV} . As indicated in Palacios-Quñonero *et al.* (2012a), if all the diagonal elements $[\hat{G}_{\text{IV}}]_{i,i}$ are negative then the fully-decentralized velocity-feedback controller in Eq.(68) admits a passive implementation by means of viscous dampers with damping constants

$$c_i = -[\hat{G}_{\text{IV}}]_{i,i}, \quad i = 1, \dots, 8 \quad (69)$$

The particular values of the damping constants that we have obtained following this approach are collected in Table 1.

As in the previous section, we have conducted a proper set of numerical simulations to illustrate the behavior of the actuation schemes AS3 and AS4, using also the full-scale North-South El Centro 1940 seismic record as ground acceleration disturbance. The obtained results are presented

in Fig. 12, where the dashed green lines with asterisks show the response of the unlinked actuation scheme AS3 with the velocity-feedback controller $u_{\text{III}}(t) = G_{\text{III}} y_{\text{III}}(t)$, the solid red lines with squares present the response of the linked actuation scheme AS4 with the velocity-feedback controller $u_{\text{IV}}(t) = G_{\text{IV}} y_{\text{IV}}(t)$, the dash-dotted blue lines with circles display the response of the linked actuation scheme AS4 with the fully-decentralized velocity-feedback controller $\hat{u}_{\text{IV}}(t) = \hat{G}_{\text{IV}} y_{\text{IV}}(t)$ and the solid black lines with triangles present the uncontrolled response. The corresponding control-effort peak-values are displayed in Fig. 13 using plain green bars for the unlinked actuation scheme AS3, red bars with dashed pattern for the linked actuation scheme AS4 with the full control matrix G_{IV} , and blue bars with crossed pattern for the linked actuation scheme AS4 with

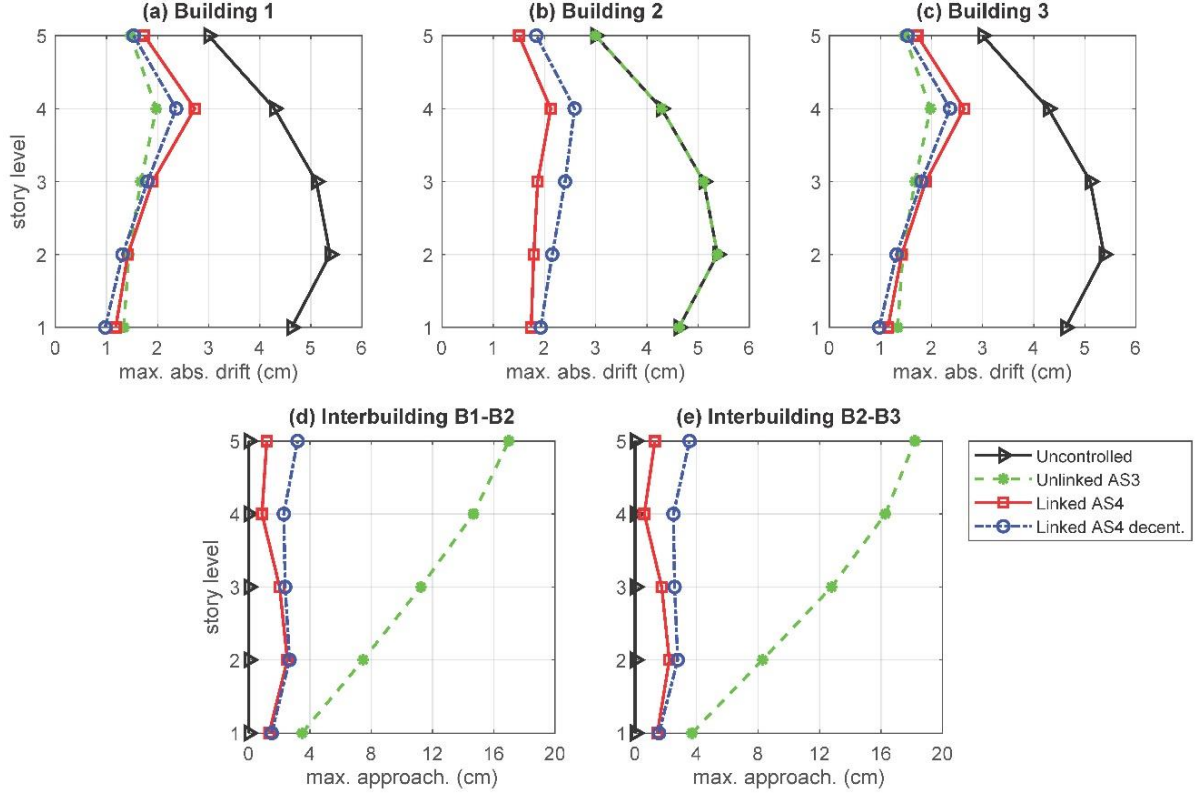


Fig. 12 Time response of the controlled three-building system corresponding to the unlinked actuation scheme AS3 with the control matrix G_{III} (dashed green line with asterisks), the linked actuation scheme AS4 with the full control matrix G_{IV} (solid red line with squares), and the linked actuation scheme AS4 with the diagonal control matrix \hat{G}_{IV} (dash-dotted blue line with circles): (a) maximum absolute interstory-drift values of building 1, (b) maximum absolute interstory-drift values of building 2, (c) maximum absolute interstory-drift values of building 3, (d) maximum interbuilding approachings between buildings 1 and 2, (e) maximum interbuilding approachings between buildings 2 and 3. The solid black line with triangles corresponds to the uncontrolled system

the diagonal control matrix \hat{G}_{IV} .

The plots in Figs. 12(a)-12(c) show that the actuation scheme AS3 attains a significant reduction of the interstory drift peak-values in the instrumented buildings $B^{(1)}$ and $B^{(3)}$, but this unlinked control configuration has null effect on the interstory drifts of the non-instrumented building $B^{(2)}$. Moreover, the plots in Figs. 12(d)-12(e) indicate that the unlinked actuation scheme AS3 has a clear detrimental effect on the pounding risk by producing large values of the maximum interbuilding approachings, which are superior to 16 cm between the buildings $B^{(1)}$ and $B^{(2)}$ and larger than 18 cm between the buildings $B^{(2)}$ and $B^{(3)}$. In contrast, the control configurations with the linked actuation scheme AS4 are able to achieve a good level of reduction in the interstory-drift peak-values of all the buildings with maximum interbuilding approachings inferior to 4 cm. Additionally, looking at the plots in Fig. 13, it can be appreciated that the positive results of the linked control configurations are attained with a moderate increase of the control-effort peak-values. It should also be highlighted the good behavior of the decentralized velocity-feedback controller defined by the diagonal control matrix \hat{G}_{IV} , which attains a level of performance similar to that

obtained by the velocity-feedback controller defined by the full matrix G_{IV} and can be implemented by a system of viscous dampers with the damping coefficients indicated in Table 1.

Remark 3. The H_∞ system norm (see Eq. (80)) of the velocity-feedback controllers defined by G_{IV} and \hat{G}_{IV} are $\gamma_{G_{IV}} = 1.1096$ and $\gamma_{\hat{G}_{IV}} = 1.1107$, respectively. This fact indicates that, compared with the non-structured centralized controller, the obtained passive control system is practically optimal.

Table 1 Damping coefficients $c_i = -[\hat{G}_{IV}]_{i,i}$ defined by the diagonal control gain matrix \hat{G}_{IV} ($\times 10^7$ Ns/m)

Building 1	Building 3	Links
$c_1 = 3.545$	$c_4 = 3.542$	$c_7 = 0.218$
$c_2 = 2.124$	$c_5 = 2.123$	$c_8 = 0.219$
$c_3 = 0.766$	$c_6 = 0.764$	

Remark 4. The LMI control design procedure used in this paper can present feasibility issues for some particular actuation schemes. Consequently, a more robust computational procedure will be necessary for a complete exploration of all possible actuation schemes.

Remark 5. All the computations in this paper have been carried out using Matlab[®] R2017b. Specifically, the LMI optimization problems have been solved with the function `mincx` included in the Robust Control Toolbox[™].

5. Conclusions

In this paper, we have investigated the design of vibration control strategies for the seismic protection of multibuilding systems formed by a row of closely adjacent identical buildings. The proposed approach considers multiactuation schemes that combine interstory actuators implemented at different levels of the buildings and interbuilding linking actuation devices. The objective of the considered control systems is to mitigate the negative seismic effects on the overall multibuilding system, including both the reduction of the vibrational response of the individual buildings and the avoidance of interbuilding collisions (pounding). Particular attention has been paid to three relevant aspects: (i) the behavior of incomplete actuation schemes that include non-instrumented buildings, (ii) the effect of unlinked actuation schemes that contain adjacent buildings with no interbuilding actuation links, and (iii) the advantages provided by properly linked actuation schemes. The main ideas have been presented by means of a system of three adjacent five-story identical buildings, for which several linked and unlinked control configurations have been designed following an advanced static output-feedback H_∞ controller design methodology. A passive control system with high-performance characteristics has also been designed by computing a fully-decentralized velocity-feedback controller. To demonstrate the response of the different control configurations, a proper set of numerical simulations has been conducted using the full-scale North-South El Centro 1940 seismic record as ground acceleration input. After considering the behavior of the different control configurations, the following points can be highlighted: (i) Linked actuation schemes with properly distributed interbuilding actuators can mitigate the vibrational response of both instrumented and non-instrumented buildings while maintaining reduced levels of pounding risk. (ii) Actuation schemes with unlinked non-actuated buildings can produce a significant increase of the pounding risk and are ineffective in reducing the vibrational response of the unlinked non-instrumented buildings. (iii) A well-balanced control action with moderate actuation-force peak-values can be obtained with a reduced set of properly distributed actuators. (iv) A remarkable performance level can be attained with passive actuation devices. Due to the simplicity and robustness of passive control systems, this can be a fact of singular relevance. (v) Decentralized control strategies with severe feedback information constraints should be considered for an effective implementation of the widely distributed actuation system.

(vi) Even for a moderate number of medium-size buildings, the overall dimension of the multibuilding system can become very large and, consequently, the computational cost can be a serious issue in designing effective controllers for a given actuation scheme. (vii) Using actuation schemes with a reduced system of interstory and interbuilding actuators leads to consider a huge variety of possible control configurations.

In summary, the observed results indicate that hybrid interstory-interbuilding actuation schemes can be used to design effective vibration control systems for adjacent buildings with similar dynamic characteristics. After the insightful perspectives provided by the three-building setup considered in this paper, a natural next step is extending the study to systems with a larger number of buildings. To carry out this research extension in a meaningful way, two main problems need to be addressed: (i) finding computationally effective controller-design strategies for large-dimension distributed actuation systems, and (ii) obtaining effective procedures for determining optimal actuation schemes. The latter is a particularly interesting and challenging problem that includes both finding optimal combinations of actuated and non-actuated buildings and obtaining optimal configurations of the distributed interstory-interbuilding actuation schemes. Finally, it should be observed that actual implementation of the proposed vibration control strategy will require 3D analyses and more accurate numerical simulations, including the effects of nonlinear elements, pounding events and soil-structure interactions.

Acknowledgments

This work was partially supported by the Spanish Ministry of Economy and Competitiveness under Grant DPI2015-64170-R/FEDER.

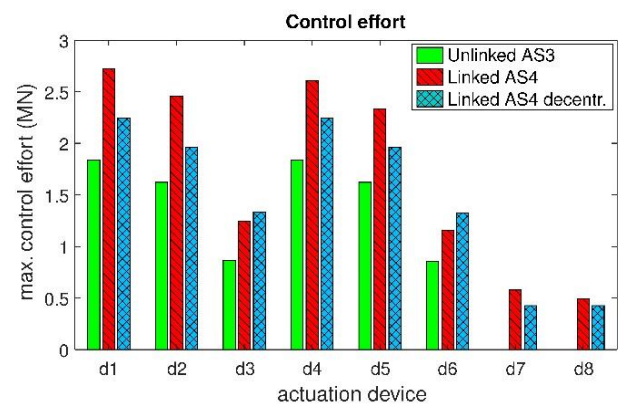


Fig. 13 Control-effort peak-values (MN) corresponding to the unlinked actuation scheme AS3 with the control matrix G_{III} (plain green bars), the linked actuation scheme AS4 with the full control matrix G_{IV} (red bars with dashed pattern), and the linked actuation scheme AS4 with the diagonal control matrix \hat{G}_{IV} (blue bars with crossed pattern)

References

- Abdullah, M.M., Hanif, J.H., Richardson, A. and Sobanjo, J. (2001), "Use of a shared tuned mass damper (STMD) to reduce vibration and pounding in adjacent structures", *Earthq. Eng. Struct. D.*, **30**(8), 1185-1201. <https://doi.org/10.1002/eqe.58>.
- Bamer, F., Shi, J. and Markert, B. (2018), "Efficient solution of the multiple seismic pounding problem using hierarchical substructure techniques", *Comput. Mech.*, **62**(4), 761-782. <https://doi.org/10.1007/s00466-017-1525-x>.
- Basili, M. and De Angelis, M. (2007), "Optimal passive control of adjacent structures interconnected with nonlinear hysteretic devices", *J. Sound Vib.*, **301**(1-2), 106-125. <https://doi.org/10.1016/j.jsv.2006.09.027>.
- Bharti, S.D., Dumne, S.M. and Shrimali, M.K. (2010), "Seismic response analysis of adjacent buildings connected with MR dampers", *Eng. Struct.*, **32**(8), 2122-2133. <https://doi.org/10.1016/j.engstruct.2010.03.015>.
- Bhaskararao, A.V. and Jangid, R.S. (2006a), "Harmonic response of adjacent structures connected with a friction damper", *J. Sound Vib.*, **292**(3-5), 710-725. <https://doi.org/10.1016/j.jsv.2005.08.029>.
- Bhaskararao, A.V. and Jangid, R.S. (2006b), "Seismic response of adjacent buildings connected with friction dampers", *B. Earthq. Eng.*, **4**(1), 43-64. <https://doi.org/10.1007/s10518-005-5410-1>.
- Bhaskararao, A.V. and Jangid, R.S. (2007), "Optimum viscous damper for connecting adjacent SDOF structures for harmonic and stationary white-noise random excitations", *Earthq. Eng. Struct. D.*, **36**(4), 563-571. <https://doi.org/10.1002/eqe.636>.
- Chinmayi, H.K. (2019), "Study on pounding of structures with soil-structure interaction effects: a review", *J. Inst. Eng. India Ser. A*, **100**(1)199-204. <https://doi.org/10.1007/s40030-018-0341-4>.
- Chopra, A.K. (2017), *Dynamics of Structures. Theory and Applications to Earthquake Engineering* (5th Ed.), Upper Saddle River, New Jersey, USA: Prentice Hall.
- Christenson, R.E., Spencer, B.F. and Johnson, E.A. (2007), "Semiactive connected control method for adjacent multidegree-of-freedom buildings", *J. Eng. Mech.*, **133**(3), 290-298. [https://doi.org/10.1061/\(ASCE\)0733-9399\(2007\)133:3\(290\)](https://doi.org/10.1061/(ASCE)0733-9399(2007)133:3(290)).
- Christenson, R.E., Spencer, B.F., Hori, N. and Seto, K. (2003), "Coupled building control using acceleration feedback", *Comput.-Aided Civ. Infrastruct. Eng.*, **18**(1), 4-18. <https://doi.org/10.1111/1467-8667.00295>.
- Cimellaro, G.P. and Lopez-Garcia, D. (2011), "Algorithm for design of controlled motion of adjacent structures", *Struct. Control Health Monit.*, **18**(2), 140-148. <https://doi.org/10.1002/stc.357>.
- Cimellaro, G.P. and Reinhorn, A.M. (2008), "Algorithm for optimal design of adjacent buildings connected by fluid viscous devices", *Proceedings of the ASCE Structures Congress 2008*, Vancouver, Canada. [https://doi.org/10.1061/41016\(314\)286](https://doi.org/10.1061/41016(314)286).
- Cundumi, O. and Suárez, L.E. (2008), "Numerical investigation of a variable damping semiactive device for the mitigation of the seismic response of adjacent structures", *Comput.-Aided Civ. Infrastruct. Eng.*, **23**(4), 291-308. <https://doi.org/10.1111/j.1467-8667.2007.00537.x>.
- Dumne, S.M., Shrimali, M.K. and Bharti, S.D. (2017), "Earthquake performance of hybrid controls for coupled buildings with MR dampers and sliding base isolation", *Asian J. Civ. Eng.*, **18**(1), 63-97.
- Fathi, F. and Bahar, O. (2017), "Hybrid coupled building control for similar adjacent buildings", *KSCE J. Civ. Eng.*, **21**(1), 265-273. <https://doi.org/10.1007/s12205-016-0708-x>.
- Impollonia, N. and Palmeri, A. (2018), "Seismic performance of buildings retrofitted with nonlinear viscous dampers and adjacent reaction towers", *Earthq. Eng. Struct. D.*, **47**(5), 1329-1351. <https://doi.org/10.1002/eqe.3020>.
- Jia, L.J., Xiang, P., Wu, M. and Nishitani, A. (2018), "Swing story-lateral force resisting system connected with dampers: novel seismic vibration control system for building structures", *J. Eng. Mech.*, **144**(2), 1-12. [https://doi.org/10.1061/\(ASCE\)EM.1943-7889.0001390](https://doi.org/10.1061/(ASCE)EM.1943-7889.0001390).
- Kharazian, A. and López-Almansa, F. (2019), "State-of-the-art of research on seismic pounding between buildings with aligned slabs", *Arch. Comput. Method. E.*, **26**(2), 327-345. <https://doi.org/10.1007/s11831-017-9242-3>.
- Khawwaja, S. and Chouw, N. (2014), "Limitations in simulation of building pounding in earthquakes", *Int. J. Protect. Struct.*, **5**(2), 123-150. <https://doi.org/10.1260/2041-4196.5.2.123>.
- Kim, H.S. (2016), "Seismic response control of adjacent buildings coupled by semi-active shared TMD", *Int. J. Steel Struct.*, **16**(2), 647-656. <https://doi.org/10.1007/s13296-016-6030-0>.
- Kurata, N., Kobori, T., Takahashi, M., Niwa, N. and Midorikawa, H. (1999), "Actual seismic response controlled building with semi-active damper system", *Earthq. Eng. Struct. D.*, **28**(11), 1427-1447. [https://doi.org/10.1002/\(SICI\)1096-9845\(199911\)28:11<C1427::AID-EQE876>3.0.CO;2-%23](https://doi.org/10.1002/(SICI)1096-9845(199911)28:11<C1427::AID-EQE876>3.0.CO;2-%23).
- Makita, K., Christenson, R.E., Seto, K. and Watanabe, T. (2007), "Optimal design strategy of connected control method for two dynamically similar structures", *J. Eng. Mech.*, **133**(12), 1247-1257. [https://doi.org/10.1061/\(ASCE\)0733-9399\(2007\)133:12\(1247\)47](https://doi.org/10.1061/(ASCE)0733-9399(2007)133:12(1247)47).
- Matsagar, V.A. and Jangid, R.S. (2005), "Viscoelastic damper connected to adjacent structures involving seismic isolation", *J. Civ. Eng. Manag.*, **11**(4), 309-322. <https://doi.org/10.1080/13923730.2005.9636362>.
- Motra, G.B., Mallik, W. and Chandiramani, N.K. (2011), "Semi-active vibration control of connected buildings using magnetorheological dampers", *J. Intel. Mat. Syst. Str.*, **22**(16), 1811-1827. <https://doi.org/10.1177/1045389X11412640>.
- Murase, M., Tsuji, M. and Takewaki, I. (2013), "Smart passive control of buildings with higher redundancy and robustness using base-isolation and inter-connection", *Earthq. Struct.*, **4**(6), 649-670. <http://dx.doi.org/10.12989/eas.2013.4.6.649>.
- Ni, Y.Q., Ko, J.M. and Ying, Z.G. (2001), "Random seismic response analysis of adjacent buildings coupled with non-linear hysteretic dampers", *J. Sound Vib.*, **246**(3), 403-417. <https://doi.org/10.1006/jsvi.2001.3679>.
- Palacios-Quinonero, F., Rossell, J.M., Rubió-Massegú, J. and Karimi, H.R. (2012c), "Structural vibration control for a class of connected multistrukture mechanical systems", *Math. Prob. Eng.*, **2012**, 1-23. <http://dx.doi.org/10.1155/2012/942910>.
- Palacios-Quinonero, F., Rubió-Massegú, J., Rossell, J.M. and Karimi, H.R. (2016), "Vibration control strategy for large-scale structures with incomplete multi-actuator system and neighbouring state information", *IET Control Theory Appl.*, **10**(4), 407-416. <https://doi.org/10.1049/iet-cta.2015.0737>.
- Palacios-Quinonero, F., Rubió-Massegú, J., Rossell, J.M. and Karimi, H.R. (2012a), "Optimal passive-damping design using a decentralized velocity-feedback H-infinity approach", *Model. Ident. Control*, **33**(3), 87-97. <https://doi.org/10.4173/mic.2012.3.1>.
- Palacios-Quinonero, F., Rubió-Massegú, J., Rossell, J.M. and Karimi, H.R. (2012b), "Semiactive-passive structural vibration control strategy for adjacent structures under seismic excitation", *J. Franklin Inst.*, **349**(10), 3003-3026. <https://doi.org/10.1016/j.jfranklin.2012.09.005>.
- Palacios-Quinonero, F., Rubió-Massegú, J., Rossell, J.M. and Karimi, H.R. (2014), "Feasibility issues in static output-feedback controller design with application to structural vibration control", *J. Franklin Inst.*, **351**(1), 139-155. <https://doi.org/10.1016/j.jfranklin.2013.08.011>.

- Palacios-Quñonero, F., Rubió-Massegú, J., Rossell, J.M. and Karimi, H.R. (2017), "Integrated design of hybrid interstory-interbuilding multi-actuation schemes for vibration control of adjacent buildings under seismic excitations", *Appl. Sci.*, **7**(4), 1-23. <https://doi.org/10.3390/app7040323>.
- Park, K.S. and Ok, S.Y. (2015a), "Hybrid control approach for seismic coupling of two similar adjacent structures", *J. Sound Vib.*, **349**, 1-17. <https://doi.org/10.1016/j.jsv.2015.03.028>.
- Park, K.S. and Ok, S.Y. (2015b), "Optimal design of hybrid control system for new and old neighboring buildings", *J. Sound Vib.*, **336**, 16-31. <https://doi.org/10.1016/j.jsv.2014.09.044>.
- Patel, C.C. and Jangid, R.S. (2010), "Seismic response of dynamically similar adjacent structures connected with viscous dampers", *IES J. Part A Civ. Struct. Eng.*, **3**(1), 1-13. <https://doi.org/10.1080/19373260903236833>.
- Patel, C.C. and Jangid, R.S. (2014), "Dynamic response of identical adjacent structures connected by viscous damper", *Struct. Control Health Monit.*, **21**(2), 205-224. <https://doi.org/10.1002/stc.1566>.
- Rubió-Massegú, J., Rossell, J.M., Karimi, H.R. and Palacios-Quñonero, F. (2013), "Static output-feedback control under information structure constraints", *Automatica*, **49**(1), 313-316. <https://doi.org/10.1016/j.automatica.2012.10.012>.
- Shahidzadeh, M.S., Tarzi, H. and Dorfeshan, M. (2011), "Takagi-Sugeno fuzzy control of adjacent structures using MR dampers", *J. Applied Sci.*, **11**(15), 2816-2822. <http://dx.doi.org/10.3923/jas.2011.2816.2822>.
- Shi, J., Bamer, F. and Markert, B. (2018), "A structural pounding formulation using systematic modal truncation", *J. Shock Vib.*, **2018**, 1-15. <https://doi.org/10.1155/2018/6378085>.
- Xu, Y.L. and Zhang, W.S. (2002), "Closed-form solution for seismic response of adjacent buildings with linear quadratic Gaussian controllers", *Earthq. Eng. Struct. D.*, **31**(2), 235-259. <https://doi.org/10.1002/eqe.107>.
- Xu, Y.L., He, Q. and Ko, J.M. (1999), "Dynamic response of damper-connected adjacent buildings under earthquake excitation", *Eng. Struct.*, **21**(2), 135-148. [https://doi.org/10.1016/S0141-0296\(97\)00154-5](https://doi.org/10.1016/S0141-0296(97)00154-5).
- Yang, Z. and Lam, E.S. (2014), "Dynamic responses of two buildings connected by viscoelastic dampers under bidirectional earthquake excitations", *Earthq. Eng. Eng. Vib.*, **13**(1), 137-150. <https://doi.org/10.1007/s11803-014-0218-0>.
- Yang, Z., Xu, Y.L. and Lu, X.L. (2003), "Experimental seismic study of adjacent buildings with fluid dampers", *J. Struct. Eng.*, **129**(2), 197-205. [https://doi.org/10.1061/\(ASCE\)0733-9445\(2003\)129:2\(197\)](https://doi.org/10.1061/(ASCE)0733-9445(2003)129:2(197)).
- Zhang, W.S. and Xu, Y.L. (1999), "Dynamic characteristics and seismic response of adjacent buildings linked by discrete dampers", *Earthq. Eng. Struct. D.*, **28**(10), 1163-1185. [https://doi.org/10.1002/\(SICI\)1096-9845\(199910\)28:10<C1163::AID-EQE860>3.0.CO;2-0](https://doi.org/10.1002/(SICI)1096-9845(199910)28:10<C1163::AID-EQE860>3.0.CO;2-0).
- Zhang, W.S. and Xu, Y.L. (2000), "Vibration analysis of two buildings linked by Maxwell model-defined fluid dampers", *J. Sound Vib.*, **233**(5), 775-796. <https://doi.org/10.1006/jsvi.1999.2735>.

Appendix A. LMI controller design procedure

In this appendix, we summarize the computational procedure used in the design of the static output-feedback H_∞ controllers presented in sections 3 and 4. A more detailed discussion can be found in Rubió-Massegú *et al.* (2013) and Palacios-Quinónero *et al.* (2014, 2016). Let us consider the state-space linear model

$$\begin{cases} \dot{x}(t) = A x(t) + B u(t) + E w(t) \\ z(t) = C_z x(t) + D_z u(t) \\ y(t) = C_y x(t) \end{cases} \quad (70)$$

where $x(t)$ is the state, $u(t)$ is the control action, $w(t)$ is the external disturbance, $z(t)$ is the controlled output, and $y(t)$ is the observed output. A static output-feedback H_∞ controller of the form

$$u(t) = G y(t) \quad (71)$$

can be computed by solving the Linear Matrix Inequality (LMI) optimization problems \mathcal{P}_1 and \mathcal{P}_2 defined below.

$$\mathcal{P}_1: \begin{cases} \text{maximize } \eta_1 \\ \text{s.t. } X > 0, \eta_1 > 0, \\ \begin{bmatrix} \text{sym}(AX + BY) + \eta_1 EE^T & * \\ C_z X + D_z Y & -I \end{bmatrix} < 0 \end{cases} \quad (72)$$

where X and Y are the optimization variables, $\text{sym}(M)$ denotes the matrix $M + M^T$ and $*$ represents the transpose of the symmetric entry.

$$\mathcal{P}_2: \begin{cases} \text{maximize } \eta_2 \\ \text{s.t. } X_Q > 0, X_R > 0, \eta_2 > 0, \\ \begin{bmatrix} E_1 + \eta_2 EE^T & * \\ E_2 & -I \end{bmatrix} < 0 \end{cases} \quad (73)$$

where E_1 and E_2 have the following form

$$\begin{aligned} E_1 &= \text{sym}(AQX_Q Q^T + ARX_R R^T + BY_R R^T) \\ E_2 &= C_z QX_Q Q^T + C_z R X_R R^T + D_z Y_R R^T \end{aligned} \quad (74)$$

X_Q , X_R and Y_R are the optimization variables; Q is a matrix whose columns contain a basis of $\text{Ker}(C_y)$; and the matrix R has the form

$$R = C_y^\dagger + Q Q^\dagger \tilde{X} C_y^T (C_y \tilde{X} C_y^T)^{-1} \quad (75)$$

where $C_y^\dagger = C_y^T (C_y C_y^T)^{-1}$, $Q^\dagger = (Q^T Q)^{-1} Q^T$ and \tilde{X} is the optimal X -matrix of the optimization problem \mathcal{P}_1 . If an optimal value $\tilde{\eta}_2$ is attained in the optimization problem \mathcal{P}_2 for the matrices \tilde{X}_Q , \tilde{X}_R and \tilde{Y}_R , then the output gain matrix

$$\tilde{G} = \tilde{Y}_R (\tilde{X}_R)^{-1} \quad (76)$$

defines a static output-feedback controller

$$u(t) = \tilde{G} y(t) \quad (77)$$

with an asymptotically stable closed-loop matrix

$$A_{\tilde{G}} = A + B \tilde{G} C_y \quad (78)$$

and the γ -value

$$\tilde{\gamma} = (\tilde{\eta}_2)^{-1/2} \quad (79)$$

provides an upper bound of the closed-loop system H_∞ norm, that is

$$\gamma_{\tilde{G}} = \sup_{\|w\|_2 \neq 0} \frac{\|z(t)\|_2}{\|w(t)\|_2} \leq \tilde{\gamma} \quad (80)$$

Appendix B. Building parameters

In this appendix, we collect the particular values of the building matrices \tilde{M} ($\times 10^5$ kg), \tilde{K} ($\times 10^8$ N/m) and \tilde{C}_d ($\times 10^5$ Ns/m) that have been used to compute the different control matrices and numerical simulations discussed in the paper.

$$\begin{aligned} \tilde{M} &= \begin{bmatrix} 2.152 & 0 & 0 & 0 & 0 \\ 0 & 2.092 & 0 & 0 & 0 \\ 0 & 0 & 2.070 & 0 & 0 \\ 0 & 0 & 0 & 2.048 & 0 \\ 0 & 0 & 0 & 0 & 2.661 \end{bmatrix} \\ \tilde{K} &= \begin{bmatrix} 2.60 & -1.13 & 0 & 0 & 0 \\ -1.13 & 2.12 & -0.99 & 0 & 0 \\ 0 & -0.99 & 1.88 & -0.89 & 0 \\ 0 & 0 & -0.89 & 1.73 & -0.84 \\ 0 & 0 & 0 & -0.84 & 0.84 \end{bmatrix} \\ \tilde{C}_d &= \begin{bmatrix} 2.602 & -0.924 & 0 & 0 & 0 \\ -0.924 & 2.196 & -0.810 & 0 & 0 \\ 0 & -0.810 & 1.995 & -0.728 & 0 \\ 0 & 0 & -0.728 & 1.867 & -0.687 \\ 0 & 0 & 0 & -0.687 & 1.274 \end{bmatrix} \end{aligned}$$

The values of the mass and stiffness coefficients have been taken from the five-story building presented in Kurata *et al.* (1999). The building damping matrix \tilde{C}_d has been computed as a Rayleigh damping matrix with 2% of relative damping in the first and fifth modes (Chopra 2017).